Catalytic methane combustion at low temperatures over YSZ-supported metal oxides: Evidence for lattice oxygen participation via the use of C18O2

Alexandre Nau, Rémy Pointecouteau, Mélissandre Richard, Thomas Belin, Fabien Can, Clément Comminges, Nicolas Bion

Catalysis Communications 180 (2023) 106704

Contents lists available at ScienceDirect

Catalysis Communications

journal homepage: www.elsevier.com/locate/catcom

Catalytic methane combustion at low temperatures over YSZ-supported metal oxides: Evidence for lattice oxygen participation via the use of $C^{18}O_2$

Alexandre Nau [a], Rémy Pointecouteau [a], Mélissandre Richard [b], Thomas Belin [a], Fabien Can [a], Clément Comminges [a], Nicolas Bion [a,*]

[a] Institut de Chimie des Milieux et Matériaux de Poitiers (IC2MP), Université de Poitiers, CNRS, TSA51106 – F86073, Poitiers Cedex 9, France
[b] Univ. Lille, CNRS, Centrale Lille, Univ. Artois, UMR 8181, UCCS – Unité de Catalyse et Chimie du Solide, 59000 Lille, France

ARTICLE INFO

Keywords:
Yttria-stabilized zirconia
Methane combustion
Lattice oxygen
Carbon dioxide
Isotopic exchange

ABSTRACT

Catalytic methane combustion was carried out over YSZ, Pd/YSZ and Rh/YSZ between 200 and 700 °C. Despite similar light-off curves for Pd/YSZ and Rh/YSZ between 200 and 450 °C, isotopic exchange experiments using CD_4 and $^{18}O_2$ revealed different behaviour of both supported catalysts regarding the activation of reactant molecules. The use of $C^{18}O_2$ isotopic gas was shown to be more appropriate than $^{18}O_2$ to evaluate the bulk oxygen mobility in YSZ at low temperatures. The exchange of gaseous CO_2 with lattice YSZ oxygen atoms, which occurs via surface hydrogen carbonate intermediate species, allowed to demonstrate the contribution of bulk oxygen atoms of YSZ in Rh/YSZ at low temperatures.

1. Introduction

Mitigating carbon dioxide emissions that cause global warming and climate alterations requires the development of renewable energy. However, until these technologies are widely deployed around the world, fossil energy will still represent a significant fraction of the energy supply chain. Among the fossil fuels (coal, oil and natural gas) which currently supply about 80% of the world's energy, the demand for natural gas is expected to increase more intensively [1]. This prevalence is related to the high energy content of natural gas (55.7 kJ g^{-1}) compared with those of coal (39.3 kJ g^{-1}) and petroleum (43.6 kJ g^{-1}) which permits to decrease the CO_2 and particulate emissions for an equivalent amount of produced heat or electricity [2]. In the automotive sector, more and more vehicles are being driven by compressed natural gas (CNG) or liquefied natural gas (LNG) worldwide. According to the Natural Gas Vehicle Knowledge Base of NGV Global (formerly known as the International Association for Natural Gas Vehicles – IANGV), >30 million of these vehicles may have been operating in 2021 (motorcycles, cars, vans, light and heavy duty trucks, buses, etc), with an annual increase of 20% in the last decade. In addition to higher fuel efficiency, replacing gasoline or diesel with CNG or LNG has also the advantage of reducing NO_x and particulate emissions [3]. Finally, the global increase in the use of methane is also encouraged by the possibility of producing synthetic natural gas (SNG or biomethane) from renewable resources by biomass gasification or biogas production associated with the methanation process [4,5]. The main problem with these utilizations of natural or synthetic methane gas in energy or transportation industries is the emission of unconverted methane throughout the world. Indeed, CH_4 is a much more powerful greenhouse gas than CO_2 (86 times higher global warming potential on a 20-year timescale), and it is the second most important anthropogenic greenhouse gas after CO_2 [6]. It is therefore crucial in the fight against climate change to limit the emissions of unburnt CH_4. One solution is the development of catalysts highly efficient in catalytic methane combustion at low temperatures, which remains a challenge due to the high stability of the C—H bond (bond energy, 450 kJ mol^{-1}).

Several families of materials have been developed for the total oxidation of methane [2,7]. The design of noble metal-based catalysts (e.g., Pd, Pt, Rh) has been widely investigated [8,9]. Because of the excessive cost of these precious and critical elements, alternative solutions based on mixed oxides perovskites-type or hexaaluminates have been also considered [10]. Regardless, Pd-based catalysts are by far the most investigated catalysts [11]. There is a kind of consensus that PdO and Pd catalyze CH_4 oxidation with different mechanisms. The methane oxidation over PdO follows a redox Mars–van Krevelen (MvK) mechanism, while Pd catalyzes the reaction via the Langmuir–Hinshelwood (LH) mechanism. In the case of LH mechanism, the reaction rate will depend on the competitive adsorption of CH_4 and O_2 on the Pd surface

* Corresponding author.
E-mail address: nicolas.bion@univ-poitiers.fr (N. Bion).

https://doi.org/10.1016/j.catcom.2023.106704
Received 28 February 2023; Received in revised form 21 May 2023; Accepted 23 May 2023
Available online 26 May 2023

[12]. In the case of MvK mechanism, CH_4 is oxidized by surface O from PdO phase which can be regenerated by the oxide support or the gaseous oxygen. Note that PdO/Pd phase transformations could also interplay in the methane oxidation activity. Whatever the mechanism is, the first C—H bond activation is usually considered as the rate-determining step [7]. Among the many studies reporting the effect of support in Pd-based catalysts [13], the behaviour of yttria-stabilized zirconia (YSZ) has rarely been investigated for methane combustion. However, YSZ has great potential for catalytic applications, as shown by Vernoux et al. [14,15] and more specifically its ability to catalyze the partial oxidation of methane (POM) [16]. Furthermore, Steghuis et al. [17] demonstrated that the combustion of CH_4 to CO_2 and H_2O via MvK oxidation reduction route with lattice oxygen sites of YSZ was the first step in the POM reaction. In more recent works, Pd/YSZ was also studied for methane oxidation under stoichiometric conditions of the POM reaction (CH_4:O_2 = 2:1) [18–20]. The utilization of $^{18}O_2$ isotope gas for the reaction clearly demonstrated the occurrence of the MvK mechanism. In these previous works, oxygen isotopic exchange experiments in a dual-bed system composed of 40 wt% $LaMnO_3$ and 60 wt% YSZ also suggested that the presence of the manganite perovskite promoted the molecular oxygen activation on the YSZ surface revealing the high oxygen mobility in YSZ at 400 °C. On the contrary, for single YSZ or Pd/YSZ (in the absence of $LaMnO_3$), the activity in the heterolytic exchange of oxygen step started at higher temperatures, above 500 °C.

In the present study, the catalytic methane combustion was carried out over YSZ, Pd/YSZ, Rh/YSZ and Rh/Al_2O_3 by using the reaction stoichiometry, CH_4:O_2 = 1:2. A specific attention was paid to the activation of both CH_4 and O_2 molecules using isotope-based characterization techniques. In particular, the $C^{18}O_2$ isotopic exchange technique combined with Diffuse Reflectance Infrared Fourier Transformed Spectroscopy (DRIFTS) was for the first time implemented on YSZ at low temperatures. To reveal the very high O mobility in YSZ crystal lattice at mild temperatures, a comparison with the widely investigated $Ce_{0.5}Zr_{0.5}O_2$ solid solution was performed below 250 °C.

2. Experimental

2.1. Materials

YSZ (Tosoh company, zirconia stabilized by 8 mol% yttrium oxide), Al_2O_3 (Axens – GOD200 – γ-alumina), ZrO_2 (Prolabo Interchim) and $Ce_{0.5}Zr_{0.5}O_2$ (provided by Rhodia) were used for the present study. Rh/YSZ, Rh/Al_2O_3 and Pd/YSZ were obtained after employing the wet impregnation method using $Rh(NO_3)_3$ and $Pd(NH_3)_2(NO_3)_2$ salt precursors. Typically, YSZ and Al_2O_3 were immersed in ultrapure water and the required amount of precursor salt was added to obtain a theoretical metal loading of 0.5 wt%. After stirring for 30 min, water was evaporated and the powder was dried at 80 °C on a sand bath, and then overnight at 110 °C in an oven under ambient air atmosphere. The powders were calcined at 700 °C under air flow for 4 h.

2.2. Catalyst characterization

The chemical composition was determined by inductively coupled plasma optical emission spectrometry (ICP-OES), using a mixture of HNO_3 and HCl to dissolve the sample. The analysis was performed in a PerkinElmer Optima 2000 DV instrument.

The BET surface area was measured by N_2 physisorption at −196 °C. The experiment was carried out in a TRISTAR 3000 Micromeritics instrument. Before the analysis, the samples (200 mg) were degassed under vacuum at 250 °C overnight.

Transmission Electron Microscopy (TEM) analysis was performed in a Jeol 2100 UHR apparatus, with 0.19 and 0.14 nm punctual and linear resolution, equipped with a LaB_6 filament. The range of X-rays emitted from the samples upon electron impact was 0–20 keV.

Oxygen Isotopic Exchange measurements were performed in a closed recycling system (70 cm^3 volume) connected to a mass spectrometer (Pfeiffer Vacuum) on the one side, and to a vacuum pump on the other side. Before each analysis, the samples (20 mg), introduced in a U-shaped reactor of 9.6 cm^3 volume were pretreated under $^{16}O_2$ flow (50 mL min^{-1}, 500 °C, 1 h) before outgassing the system under primary vacuum for 30 min. Then, the sample was cooled down to the temperature of the experiment. Isothermal Oxygen Isotopic Exchange (IOIE) experiments were performed to determine kinetic parameters of the exchange process at selected temperatures. Temperature-programmed Oxygen Isotopic Exchange (TPOIE) experiments were also carried out to follow the oxygen exchange activity as a function temperature. Typically 55 mbar of pure $^{18}O_2$ (≥ 99 at.%, ISOTEC) was admitted into the reactor at the selected temperature for IOIEs test or at 200 °C followed by an increase of the temperature to 700 °C (ramp rate = 2 °C min^{-1}) for TPOIE tests. Each isotopologue concentration was analyzed by monitoring with mass spectrometry the *m/z* signals: 32 ($^{16}O_2$), 34 ($^{18}O^{16}O$), and 36 ($^{18}O_2$). The m/z = 28 signal was also monitored to check possible entrance of air in the system.

The relationships to calculate the atomic fraction of $^{18}O_2$ at time t (α_g^t) (Eq. 1) and the number of oxygen atoms exchanged (N_e) (Eq. 2) are indicated below, where α_g^0 is the initial atomic fraction of $^{18}O_2$ in the gas phase, w (g) is the weight of catalyst, and N_g is the total number of O atoms in the gas phase:

$$\alpha_g^t = \frac{1/2P_{34}^t + P_{36}^t}{P_{32}^t + P_{34}^t + P_{36}^t} \quad (1)$$

with P_{32}^t, P_{34}^t and P_{36}^t being the partial pressures at time t of $^{16}O_2$, $^{18}O^{16}O$ and $^{18}O_2$ isotopologues, respectively.

$$N_e = \left(\alpha_g^0 - \alpha_g^t\right) N_g \frac{1}{w} \quad (2)$$

It is also possible to determine the number of exchangeable oxygen atoms, N_s when the gas/solid equilibrium, corresponding to similar ^{18}O ratio in the gas-phase and the solid sample is reached (Eq. 3):

$$N_s = \frac{N_e}{\alpha_g^*} = N_g\left(\frac{1-\alpha_g^*}{\alpha_g^*}\right) \quad (3)$$

where the α_g^* value corresponds to the relative concentration of ^{18}O atoms in the gas-phase when the gas/solid equilibrium is reached [21].

Additional IOIE and TPOIE experiments were performed by substituting $C^{18}O_2$ (97% purity, ISOTEC) for $^{18}O_2$ as the labelled molecule. The experimental protocol applied was maintained and the following *m/z* values were monitored by mass spectrometry as a function of time: 44 ($C^{16}O_2$), 46 ($C^{18}O^{16}O$), and 48 ($C^{18}O_2$).

Infrared spectra were collected during the IOIE experiments with $C^{18}O_2$ using a ^{18}O labelling-DRIFTS coupling setup described elsewhere [20]. The DRIFTS cell was placed in a Bruker (Equinox 55) IR spectrometer with a MCT (Mercury–Cadmium–Telluride) detector. Spectra were collected in the range of 400 to 4000 cm^{-1} and accumulating 64 scans with a spectral resolution of 4 cm^{-1}. Reference spectra were recorded using a KBr powder sample registered at ambient temperature under primary vacuum and at the temperatures of the IOIE experiments.

Diffusion coefficients were estimated by fitting the transient response curves of heterolytic exchange with CO_2. As detailed by Klier et al. [22] and Muzykantov et al. [23], three types of isotope exchange were considered in this numerical approach:

(i) homomolecular exchange type (named r_0) with no participation of atoms from the solid: $^{18}O_2 + {}^{16}O_2 \rightleftarrows 2\,{}^{16}O^{18}O$,
(ii) heterolytic exchange (named r_1) between one atom from the gas phase and one atom from the solid. Oxygen atoms from the solid surface (O_s) were involved in this reaction: $^{18}O_2 + {}^{16}O_s \rightleftarrows {}^{16}O^{18}O + {}^{18}O_s$ and $^{16}O^{18}O + {}^{16}O_s \rightleftarrows {}^{16}O_2 + {}^{18}O_s$, and

(iii) 2-atoms heterolytic exchange (named r_2) between gas molecule O_2 and the oxygen atoms from the solid: $^{18}O_2 + 2^{16}O_s \rightarrow {}^{16}O_2 + 2^{18}O_s$; $^{16}O^{18}O + 2^{16}O_s \rightarrow {}^{16}O_2 + {}^{16}O_s + {}^{18}O_s$ and $^{16}O^{18}O + 2^{18}O_s \rightleftarrows {}^{18}O_2 + {}^{16}O_s + {}^{18}O_s$.

In general, the exchange mechanisms were not similar to the exchange types since some mechanism variants may be formulated for isotopic exchange types. Indeed, even if the CO_2 isotopic exchange mechanisms were different from those of O_2 exchange, identical oxygen exchange types were considered in these experiments.

A model derived from Klier et al. [24] was used to describe the main processes, namely, both surface exchange and bulk isotope diffusion process steps were involved in the oxide oxygen exchange rate. Sample particles were modelled as one-dimension spherical particles of radius L (m). The oxygen amount in the sample (N_{ox} atoms) was defined as the sum of atomic oxygen in the solid (N_v atoms) except that on the surface (N_s atoms), and which was determined using crystallographic considerations. The homomolecular exchange reaction in the gas phase (r_0 constant rate, s^{-1}) was considered as negligible due to the low temperature used for the isothermal isotopic exchange experiments. Description of the dynamics of oxygen exchange via this model is as follows:

(i) In the gas phase, the variation of the ^{18}O fraction, α_g was related to the adsorbed amount of oxygen on the oxide following the relationship:

$$\frac{\partial \alpha_g^t}{\partial t} = b \cdot r_H \cdot \left(\alpha_s^t - \alpha_g^t\right) \quad (4)$$

where b is the ratio of the number of oxygen atoms at the surface of the solid, N_s compared to the gas phase, N_g, r_H is the rate constant describing the heteroexchange reactions ($r_H = 0.5r_1 + r_2$), and α_s^t is the ^{18}O fraction at the oxide surface.

(ii) At the gas/solid interface, the oxygen atoms were assumed to be identical (homogeneous surface) and the number of adsorbed oxygen was considered negligible compared to the number of oxygen atoms in the oxide surface. The variation of the atomic fraction of ^{18}O at the surface of the sphere, α_s^t was given by the quantity adsorbed on this surface from which the quantity which diffuses in the solid was subtracted (Eq. 5):

$$\frac{\partial \alpha_s^t}{\partial t} = r_H \cdot \left(\alpha_g^t - \alpha_s^t\right) - 3 \cdot b_s \cdot \frac{D}{L} \cdot \left.\frac{\partial \alpha}{\partial R}\right|_{R=L} \quad (5)$$

where b_s is ratio between N_v, the oxygen atomic amount in the solid except the surface, and N_s, the oxygen atomic amount at the surface. D ($m^2\ s^{-1}$) is the effective diffusion coefficient inside the solid oxide particle.

(iii) In the solid, the second Fick's law was considered for the bulk oxygen diffusion process (Eq. 6):

$$\frac{\partial \alpha}{\partial t} = \frac{D}{R^2} \cdot \frac{\partial}{\partial R} \cdot \left(R^2 \frac{\partial \alpha}{\partial R}\right) \quad (6)$$

where α is the ^{18}O fraction in the solid except the surface, D is the already defined diffusion coefficient, and R is the coordinate along the oxide particle radius (m). The initial conditions were set as a known amount of ^{18}O oxygen in the gas phase and none at the surface or in the oxide (the natural abundance of ^{18}O in oxide was neglected). The boundary conditions were expressed by a finite concentration at the core of the oxide particle:

$$\left.\frac{\partial \alpha}{\partial R}\right|_{R=0} = 0 \quad (7)$$

and by an identical atomic fraction at the surface and in the oxide volume:

$$\alpha|_{R=L} = \alpha_s \quad (8)$$

Using a homemade software written in Python, the system of three equations (in adimensional forms, Eqs. 4–6) was solved by the method of lines (70 points along the characteristic length L were used) [25]. Fraction profiles ($C^{16}O_2$, $C^{16}O^{18}O$ and $C^{18}O_2$ in the gas phase) as a function of time were then obtained from the numerical solution of this system. The physicochemical parameters were determined from the experimental gas fraction transient curves using the global particle swarm optimization method (PSO) [26]. This method is a very popular optimization which has been successfully applied to the kinetic parameters' estimation problem [27]. The following parameters were applied: 20 swarm particles over 1000 iterations, and 1×10^{-8} as minimal change in the swarm's best objective value was used. The sum of squared residuals was used as the minimizing function:

$$\sigma = \sum_{i=1}^{n} \left(x_{44}^{exp} - x_{44}^{calc}\right)^2 + \sum_{i=1}^{n} \left(x_{46}^{exp} - x_{46}^{calc}\right)^2 + \sum_{i=1}^{n} \left(x_{48}^{exp} - x_{48}^{calc}\right)^2 \quad (9)$$

where x_{44}, x_{46} and x_{48} are the mole fractions of oxygen molecules of three different isotopic compositions: $C^{16}O_2$, $C^{16}O^{18}O$ and $C^{18}O_2$ in the gas phase; indexes exp and *calc* are related to experimental and calculated values of oxygen mole fractions.

Temperature-programmed homomolecular exchange of methane was performed to evaluate the ability of the catalyst to activate the C—H bond. The gas mixture was composed of CH_4 and CD_4 in *quasi* equal proportions, with a total pressure of 60 mbar and the temperature of exchange was increased from 200 to 700 °C.

2.3. Methane combustion activity measurements

The experiments were carried out in a fixed-bed quartz reactor at atmospheric pressure. The samples (75 mg) were diluted with 450 mg SiC to avoid hot spot or temperature gradients. Samples were in-situ treated at 200 °C under He for 30 min (30 mL min^{-1}) before introduction of the reactant mixture (CH_4:O_2:He molar ratio equal to 1:2:14; total flowrate = 200 mL min^{-1}). After stabilization of the reacting mixture composition, the catalytic test started with a first temperature ramp (5 °C min^{-1}) from 200 °C to 700 °C. At the end of the ramp, the reactor was cooled to 200 °C under reaction mixture gas flow before repeating a second ramp from 200 to 700 °C. The comparison of light-off curves was based on the second ramp (the first ramp served as the stabilization of the catalytic behaviour). The exit gas flow from the reactor went through a double glass wall condenser connected to a cooling circulator for H_2O removal, and the composition of it was analyzed by two gas chromatographs (VARIAN GC3900) fed by He as carrier gas: one equipped with a FID detector and a Porapak Q column (i.d. = 6 mm, L = 0.3 m) dedicated to CH_4 analysis, while the other one was equipped with a TCD detector and a Altech® CTR I column capable of separating H_2, O_2, CO_2, N_2, CH_4 and CO. With these operational conditions, only CO_2 was detected as product of the oxidation reaction, indicating that the conversion of CH_4 is directly linked to the combustion reaction (no secondary reactions like partial oxidation or decomposition were found). The conversion of CH_4 is given by Eq. (10).

$$X_{CH_4} = \frac{(F_{CH_4})_{feed} - (F_{CH_4})_{exit}}{(F_{CH_4})_{feed}} \times 100 \quad (10)$$

3. Results and discussion

3.1. Catalytic behaviour in methane combustion

The catalytic performance in methane combustion on YSZ, Rh/YSZ and Pd/YSZ solids were compared in terms or light-off experiments between 200 and 700 °C under a reaction mixture consisted of CH_4:O_2:

He = 1:2:14 (total flowrate = 200 mL min^{-1}). Commercial YSZ consisted of 8 mol% Y_2O_3 in zirconia as investigated in previous works [20,28]. After wet impregnation synthesis of catalysts, the metal loadings of Rh/YSZ and Pd/YSZ were found to be 0.46 and 0.43 wt%, respectively, close to the theoretical value of 0.50 wt%. The impregnation method slightly decreased the specific surface area of YSZ from 13 m^2 g^{-1} to 11 and 10 m^2 g^{-1} after deposition of Rh and Pd, respectively (Table 1).

Light-off curves of the catalytic combustion are presented in Fig. 1. For single YSZ, the CH_4 conversion starts to increase above 550 °C and reaches 19% at 700 °C. As a non-reducible metal oxide, the low activity of YSZ at mild temperatures was expected and already reported for the catalytic partial oxidation of methane [29]. The YSZ-supported metal catalysts exhibit much better performance. In the region below 450 °C, the light-off curves are very similar for Rh/YSZ and Pd/YSZ with CH_4 conversion starting around 250 °C to reach 73% for Rh/YSZ and 68% for Pd/YSZ at 450 °C. The T_{50} values corresponding to the temperature required to have 50% conversion are 416 and 424 °C for Rh- and Pd-based catalysts, respectively. The uncertainty of the measurements estimated to be lower than 6% did not permit to differentiate the two catalysts in this range of temperatures. In the region above 450 °C, the catalytic behaviour of the two samples differs drastically. In the case of Rh/YSZ, the conversion of CH_4 continuously increases to achieve 100% at 536 °C, with full conversion maintained up to 700 °C. In the case of Pd/YSZ, the conversion reaches a maximum of 88% at 540 °C before decreasing to 68% at 685 °C (same conversion as obtained at 450 °C). Between 685 and 700 °C, the decrease of conversion is practically zero, and a slight increase is rather observed. The same evolution of conversion was observed in the first light-off curve and during the cooling step from 700 to 200 °C before the second light-off experiment was conducted, results of which are shown in Fig. 1. A sintering of PdO_x active sites at high temperatures to explain this behaviour is excluded because it would lead to an irreversible deactivation of the catalyst.

The deactivation of supported Pd catalysts at high temperature in methane combustion is a well reported phenomenon for other supports than YSZ. In 1992, Farrauto et al. [30] demonstrated that the activity of Pd/Al_2O_3 for methane combustion under large excess of oxygen was maximum at 600 °C and reduced above 680 °C due to PdO decomposition (active phase) to palladium metal [30]. The same study showed that the high conversion observed above 700 °C was due to γ-alumina as well. By analogy, the decrease of conversion observed on Pd/YSZ above 540 °C might be explained by the decomposition of PdO which occurs at quite low temperatures because of the stoichiometric conditions of the combustion used in the present study (CH_4:O_2 = 1:2). PdO decomposition on YSZ would be expected at higher temperatures under large excess of oxygen as it has been observed in a recent study on Pd/YSZ or associated to $CaTi_{0.7}Fe_{0.3}O_3$-perovskite in a dual catalytic bed [31].

Rh-based catalysts have been less documented for methane combustion [8,32]. They were mainly investigated to abate the unburned methane from natural-gas engines usually in association with Pt and/or Pd inside the catalytic converters of vehicles [33]. In a study comparing alumina-supported metal catalysts, Oh et al. [34] reported that the methane oxidation activity decreased in the order Pd > Rh > Pt under oxidizing conditions. However, in this study a small concentration of CO was added in the stream to simulate exhaust gases of natural-gas vehicles. To the best of our knowledge, the activity of Rh/YSZ catalyst for methane combustion was not previously reported.

Table 1
Metal loading and specific surface area of investigated catalysts.

Catalyst	Crystallographic structure	Metal loading (wt %)	Specific surface area (m^2 g^{-1})
YSZ	Cubic	–	13
Rh/YSZ		0.46	11
Pd/YSZ		0.43	10
Rh/Al_2O_3		0.56	191
ZrO_2	Cubic	–	< 1
$Ce_{0.5}Zr_{0.5}O_2$	Tetragonal	–	61

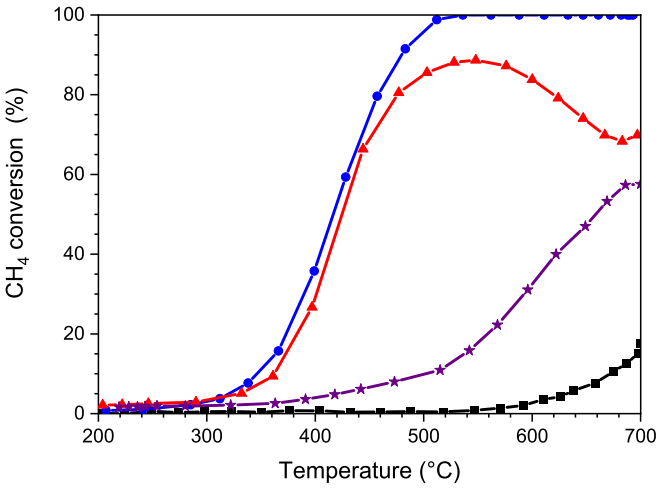

Fig. 1. Light-off curves of methane combustion (CH_4:O_2:He = 1:2:14) for YSZ (black line with squares), Rh/YSZ (blue line with circles), Pd/YSZ (red line with triangles) and Rh/Al_2O_3 (purple line with stars). (For interpretation of the references to colour in this figure legend, the reader is referred to the web version of this article.)

In an effort to highlight the specific behaviour of YSZ support, the catalytic performance of Rh/YSZ catalyst was compared with that of Rh/Al_2O_3 catalyst. The metal loading and specific surface area of Rh/Al_2O_3 were 0.56 wt% and 191 m^2 g^{-1}, respectively (Table 1). In addition, the same impregnation method was used in the catalyst's preparation stage. To verify the possible influence of the difference in the specific surface areas between Al_2O_3 and YSZ supports on the metal dispersion, an estimation of the mean metal particle size was determined by TEM measurements. Examples of TEM pictures are presented in Fig. 2a and Fig. 2b for Rh/Al_2O_3 and Rh/YSZ, respectively. From these analyses, the mean size of Rh particles was estimated to be 1.7 nm (based on 216 particles) when supported on YSZ. In the case of Al_2O_3, the size of Rh particles varied between 1 and 2 nm with a number density of 1-nm metal particles higher on Al_2O_3 than YSZ. It is worth noting that on the larger surface γ-alumina, more sensitive to the electron beam, the analysis using large magnification was less precise. However, one can reasonably conclude that both samples exhibit nearly the same mean metal particle size.

The light-off curve obtained for the Rh/Al_2O_3 catalyst is also presented in Fig. 1 for comparison. It is clearly illustrated the beneficial effect of YSZ support since the T_{50} observed at 660 °C is 240 °C above the T_{50} obtained for Rh/YSZ. Moreover, the maximum of conversion does not exceed 57% on Rh/Al_2O_3, while 100% conversion was reached at 536 °C on Rh/YSZ. Although the possibility of Rh particle migration into the alumina lattice cannot be ruled out [35], these results demonstrate the efficacy of YSZ mixed oxide as support for Rh particles in the methane combustion reaction.

The behaviour of Pt/YSZ was investigated for propane deep oxidation, and the utilization of gas-phase $^{18}O_2$ permitted to demonstrate that the CO_2 product mainly contained lattice oxygen species of the YSZ support [36]. The participation of O lattice atoms from YSZ in the methane oxidation reaction was also observed by us recently on Pd/YSZ using ^{18}O labelling-DRIFTS coupling experiments [20]. It was then interesting to investigate the behaviour of lattice O atoms in Rh/YSZ catalyst.

3.2. Oxygen isotopic exchange studies

Temperature-programmed Oxygen Isotopic Exchange (TPOIE) experiments were performed to compare the ability of lattice O atoms from

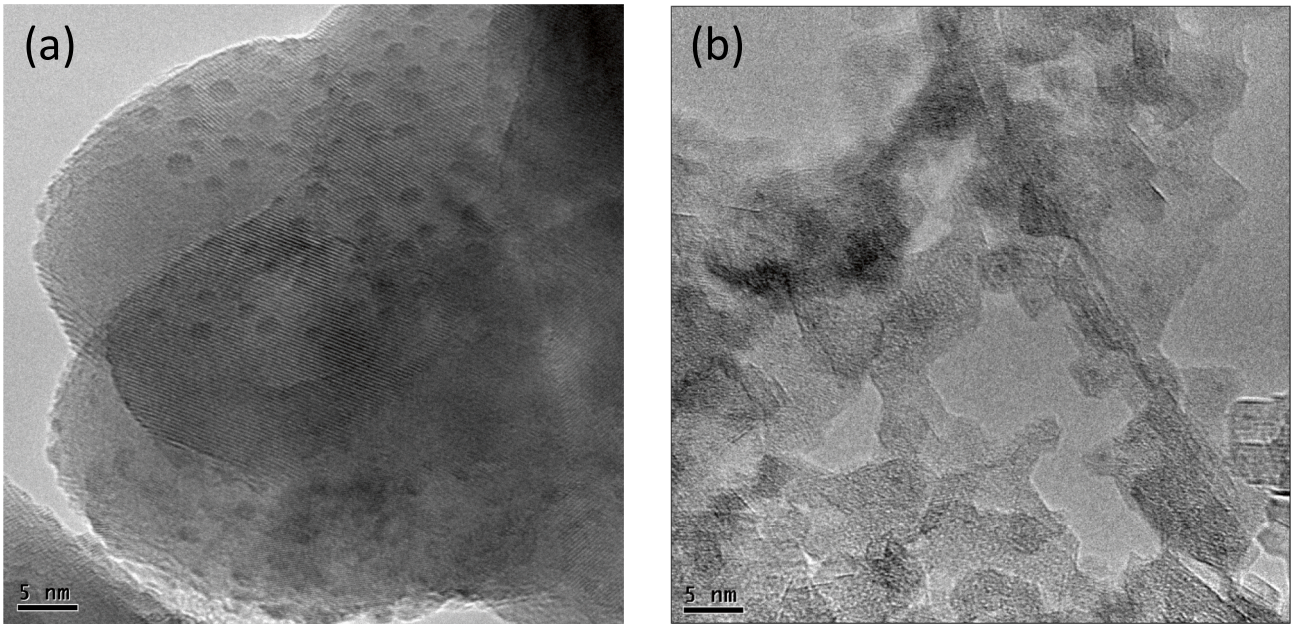

Fig. 2. TEM images of calcined (a) Rh/YSZ and (b) Rh/Al_2O_3 catalysts.

YSZ, Pd/YSZ and Rh/YSZ to exchange with molecular O_2 from the gas-phase in the temperature range between 200 and 700 °C. The obtained results are presented in Fig. 3 where the number of atoms exchanged (N_e values) are plotted as a function of the temperature. Considering the pressure of $^{18}O_2$ and the weight of sample used in the closed recycling system, the value of 5×10^{21} at. O g^{-1} for N_e corresponds to the expected value for gas/solid equilibrium in the case of a complete exchange of lattice O atoms. It also represents 53% of the total number of O atoms in the solid. As already reported in [18,20], the presence of Pd has little influence on the $^{18}O/^{16}O$ heterolytic exchange activity of YSZ. Indeed, the exchange reaction process occurs above 500 °C, and the N_e values drastically increased between 600 and 700 °C for both YSZ and Pd/YSZ. At 700 °C, the absence of plateau means that the gas/solid equilibrium was not reached. At this temperature, 28% and 41% of O atoms from YSZ and Pd/YSZ, respectively, are exchanged, showing that at high temperatures a slight enhancement of the exchange rate is observed due to the presence of Pd. The behaviour of Rh/YSZ differs drastically, with an exchange activity starting at 300 °C, almost 200 °C lower than for Pd/YSZ. Moreover, the N_e curve reached a plateau at 600 °C close to the value of 5×10^{21} at O g^{-1}, meaning that the bulk diffusion of O inside the YSZ is sufficiently high to enable complete exchange of the lattice O atoms of YSZ. The beneficial impact of the rhodium on the exchange activity was already established with TPOIE experiments performed on the alumina-supported Rh catalyst [37]. However, it was clearly showed that the main role of rhodium was to decrease the temperature range of surface oxygen species exchanged by enhancing O_2 activation. The N_e curve observed for Rh/YSZ (blue line with circles in Fig. 3) shows that the exchange is not limited to the surface but implies the participation of bulk oxygen atoms of YSZ. This result reinforces the data reported in our previous study related to the oxygen exchange activity of a dual bed of $LaMnO_3$-YSZ. In that study we concluded that the diffusion of lattice oxygen in YSZ was not the limiting parameter of the gas/solid oxygen exchange activity at mild temperatures (below 550 °C) [18]. Indeed, the absence of exchange activity for single YSZ below 500 °C is due to the lack of energy at this temperature for the activation of O_2 on the mixed oxide surface. Contrary to palladium, the rhodium particles activate the dissociation of molecular oxygen, which is considered as the first step of oxygen exchange mechanism.

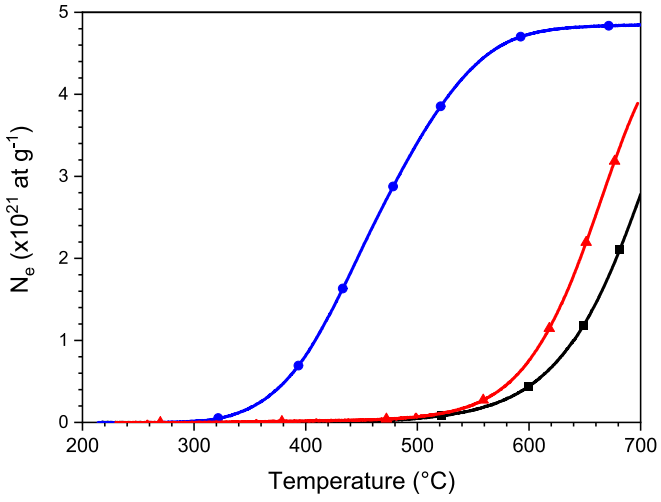

Fig. 3. Evolution of the number of exchanged atoms (N_e) with temperature during TPOIE experiments with $^{18}O_2$ on YSZ (black line with squares), Rh/YSZ (blue line with circles) and Pd/YSZ (red line with triangles). (For interpretation of the references to colour in this figure legend, the reader is referred to the web version of this article.)

The correlation between light-off curves of methane combustion and exchange activity curves show that the activation and diffusion of oxygen would not play the same role if any for the Rh/YSZ and Pd/YSZ catalysts, since similar catalytic performances were obtained on both materials below 450 °C (Fig. 1) with various O_2 exchange activities (Fig. 3). Despite the difference of operating conditions between catalytic tests (fixed bed reactor under flow of reactant mixture at atmospheric pressure) and TPOIE experiments (U-shaped reactor in a closed recycling system at 55 mbar), one can speculate that gaseous molecular oxygen interacts with lattice oxygen of Rh/YSZ during the combustion reaction, while O_2 activation is not directly taking place on the Pd/YSZ surface. Another limiting step for the methane combustion is linked to the very stable C—H bond in CH_4. Because of the relative inertness of methane, one of the most efficient routes for its activation is the homolytic C—H bond cleavage [38]. A technique which is rarely used to characterize the ability of the catalyst to activate the C—H cleavage is that of CD_4/CH_4 homomolecular exchange reaction to be described next.

3.3. CD_4/CH_4 homomolecular exchange reaction studies

Since the pioneering work of Kemball [39] on methane-deuterium exchange over platinum group catalytic films, CH_4/D_2 experiments has been widely used for describing the methane activation mechanism in a CH_4–D_2-solid system [40]. In a similar way used for the oxygen equilibration reaction ($^{18}O_{2(g)} + {}^{16}O_{2(g)} = 2\,{}^{18}O^{16}O_{(g)}$), which is carried out to characterize the ability of catalytic surface to dissociatively adsorb molecular oxygen [41], methane equilibration was implemented ($CD_{4(g)} + CH_{4(g)} = 2CD_2H_{2(g)}$) to investigate the C—H activation on YSZ, Pd/YSZ and Rh/YSZ. This homomolecular isotopic exchange reaction, in which a mixture of CD_4 and CH_4 is scrambled over the catalytic surface, will hereafter be denoted as the equilibration reaction. The analysis by mass spectrometry is complex because of the numerous (m/z) signals expected for the formation of possible CD_xH_{4-x} isotopic species during equilibration reaction, but also of the associated signals due to the fragmentation in the ionisation chamber. The analysis of the C—H activation was focused on the observation of the evolution of the intensity of the $m/z = 19$ signal. This signal enables to follow the formation of CD_3H isotope produced by CD_4/CH_4 equilibration and is not dependent on other isotopic species evolution contrary to m/z = 18,17,16, 15, 14 or 13 [42]. Fig. 4 shows a comparison of the evolution of m/z = 19 signal as a function of temperature for YSZ, Pd/YSZ and Rh/YSZ catalysts during the CD_4/CH_4 homomolecular exchange. The behaviour of the intensity of m/z = 29 signal vs T curves is clearly different among the three solids. The formation of CD_3H appears at 300 °C on Pd/YSZ, which is the starting temperature for methane combustion on this sample (Fig. 1). The same isotope is produced at 400 °C for Rh/YSZ, while it occurs at a much higher temperature for YSZ. It is worth noting that signals expected for the formation of oxidation products (m/z = 44 for CO_2 and m/z = 28 for CO) were also monitored. In the absence of molecular O_2 in the gas phase, the CO_2 production was detected for Pd/YSZ and Rh/YSZ catalysts in very low concentrations (from 275 to 600 °C with a maximum at 415 °C). The formation of CO was observed after the appearance of CD_3H isotope with a continuous increase from 400 °C for Pd/YSZ and Rh/YSZ, and from 480 °C for YSZ. In a study on Pd/ZrO_2, Au-Yeung et al. [43] reported that the rate of isotopic CH_4–CD_4 equilibration was much smaller than the rate of methane combustion [43] after using $CD_4/CH_4/O_2$ mixture, and they concluded that the C—H bond activation is irreversible during CH_4 combustion on PdO_x. Here, the exchange rate cannot be directly compared because of the differences between exchange and combustion tests. However, one can speculate a similar behaviour between Pd/ZrO_2 and Pd/YSZ. The same conclusion seems also reasonable for Rh/YSZ for which the equilibration reaction appears 100 °C higher than the combustion reaction. The additional conclusion is that the C—H bond is more efficiently activated on Pd/YSZ than on Rh/YSZ in the absence of molecular oxygen in the gas mixture, while the opposite is observed for the O_2 exchange experiments (Fig. 3). Based on the results obtained in $^{18}O_2/^{16}O_2$ exchange and CD_4/CH_4 equilibration, it is obvious that the lattice oxygen of YSZ in Rh/YSZ catalyst are involved in the combustion of CH_4 following a MvK mechanism for which only surface oxygen are suspected to participate to the oxidation of metal oxide support [44].

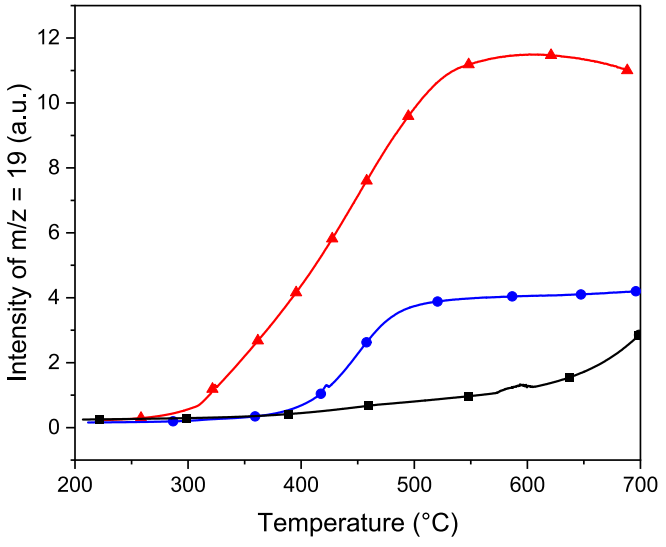

Fig. 4. Evolution of the mass spectrometry $m/z = 19$ signal intensity, characteristic of the CD_3H isotope, produced by CD_4/CH_4 equilibration on YSZ (black line with squares), Rh/YSZ (blue line with circles) and Pd/YSZ (red line with triangles). (For interpretation of the references to colour in this figure legend, the reader is referred to the web version of this article.)

Knowing the good ionic conductivity of YSZ, diffusion of bulk oxygen atoms could be a key parameter for the methane oxidation activity of Rh/YSZ. To have information about the possibility of YSZ's bulk oxygen atoms to be involved in the catalytic methane combustion, additional isotopic oxygen exchange studies were carried out with ^{18}O-labelled carbon dioxide, which is a product of the combustion reaction.

3.4. $C^{18}O_2/^{16}O$ exchange reaction studies

Diffusion of oxygen has been widely investigated in YSZ mixed oxides as electrolytes of solid oxide systems (SOFC, SOEC or membrane) [45]. For such applications, YSZ is annealed at very high temperatures (~1300 °C) to be sufficiently dense and avoid gas-phase diffusion. Furthermore, the effective diffusivity is usually measured for $T > 600$ °C. Although rarely used, Kurumchin and Perlliev [46] reported that exchange rates with $C^{18}O_2$ largely exceeds the exchange rates with $^{18}O_2$. For instance, at 800 °C the exchange rate of CO_2 differs from that of O_2 by a factor of 600 for the composition 0.9 ZrO_2 + 0.1 Y_2O_3. On divided YSZ, we demonstrated previously that oxygen exchange rates at mild temperatures were restricted by the dissociative adsorption of molecular oxygen. It is therefore interesting to investigate the oxygen exchange rates with $C^{18}O_2$ tracer. This study was carried out on single YSZ to avoid CO_2 dissociation, which can occur at low temperatures on Rh or Pd-supported catalysts [47,48]. The earlier described TPOIE protocol (Section 2.2) was used by substituting $C^{18}O_2$ for $^{18}O_2$. Fig. 5a shows the evolution of the isotopic distribution composition during the TPOIE with $C^{18}O_2$. Contrary to the behaviour observed with $^{18}O_2$, the exchange reaction between gas phase CO_2 and lattice ^{16}O of YSZ is very rapid at 200 °C. An important decrease of the partial pressure of $C^{18}O_2$ is observed between 200 and 250 °C correlated to the successive production of $C^{18}O^{16}O$ and $C^{16}O_2$ isotopes. The evolution of the number of exchanged atoms was determined from the curves of CO_2 isotopologues and reported in Fig. 5b (full line). The plateau observed starting at 250 °C towards higher temperatures indicates that the gas/solid equilibrium is reached at this temperature, and that the N_e value calculated for this plateau means that all the lattice ^{16}O atoms can be considered as participating in the exchange process. These results demonstrate that the diffusion of bulk oxygen atoms of YSZ is high at 200 °C. For comparison, the same experiment was carried out on pure ZrO_2 (dashed line in Fig. 5b) showing that below 350 °C, the exchange activity for $C^{18}O_2/^{16}O$ is very low.

The difference of activity in the exchange process between lattice oxygen and either O_2 or CO_2 can be attributed to differences in mechanism and kinetics of the exchange process: (i) a dissociative mechanism with RDS that of O_2 dissociation step, and (ii) an associative mechanism via the formation and decomposition of carbonate complex (CO_3^{2-}) formed on the oxide surface in the case of the exchange with CO_2. Other studies performed on acidic oxides (SiO_2, γ-Al_2O_3, zeolite) [49] or basic metal oxides (CaO, MgO, ZnO and ZrO_2) [50] have shown the formation of carbonate species by infrared spectroscopy during the exchange of oxygen with $C^{18}O_2$. The exchange mechanism would start with the CO_3^{2-} adsorbed species formation via the interaction of $C^{18}O_{2(g)}$ with an

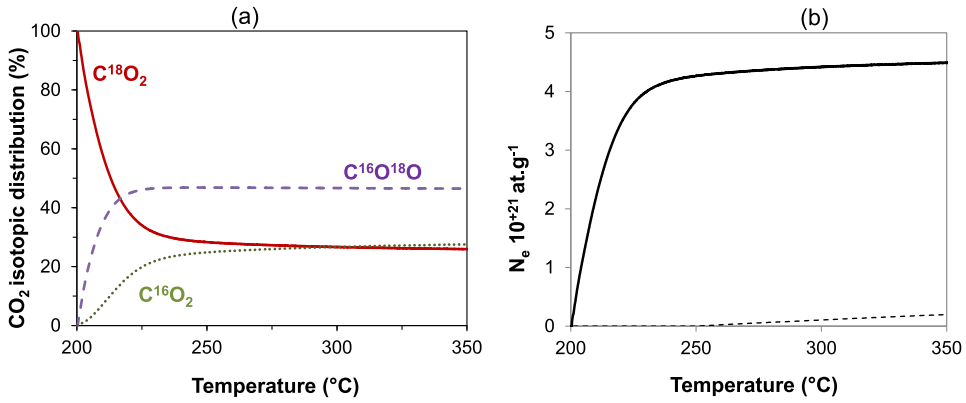

Fig. 5. Heterolytic exchange of gaseous $C^{18}O_2$ with lattice ^{16}O atoms as a function of time: (a) evolution of the CO_2 isotopic concentration distribution on YSZ; (b) evolution of the number of O-exchanged atoms for YSZ (full line) and ZrO_2 (dashed line).

oxygen atom of the solid $^{16}O^{2-}_{(s)}$ (Eq. 11). The species formed will then either decompose or react further with CO_2 to form the $C^{16}O^{18}O$ isotope in the gas phase (Eqs. 12 and 13). The latter species can follow the same mechanistic steps leading eventually to $C^{16}O_2$(g).

$$C^{18}O_{2(g)} + {}^{16}O^{2-}{}_{(s)} \rightleftharpoons C^{18}O_2{}^{16}O^{2-}{}_{(ads)} \text{ (Formation)} \quad (11)$$

$$C^{18}O_2{}^{16}O^{2-}{}_{(ads)} \rightleftharpoons C^{18}O^{16}O_{(g)} + {}^{18}O^{2-}{}_{(s)} \text{ (Decomposition)} \quad (12)$$

$$C^{18}O_{2(g)} + C^{18}O_2{}^{16}O^{2-}{}_{(ads)} \rightleftharpoons C^{18}O^{16}O_{(g)} + C^{18}O_3{}^{2-}{}_{(ads)} \quad (13)$$

These mechanistic steps (Eqs. 11–13) are consistent with the evolution of the isotopic distribution observed in Fig. 5a. To identify the nature (chemical structure) of the intermediate species implied in the exchange mechanism with CO_2 on YSZ, the isotopic exchange was performed in a DRIFTS cell equipped with a Harrick environmental chamber served as the micro-reactor. This coupling between DRIFTS and isotopic exchange technique was carefully described in a previous study [20]. A 130-mg sample was necessary to fill in the crucible (sample holder)of the DRIFTS cell instead of 20 mg used in the classical IOIE experiment with a U-shaped micro-reactor. Before monitoring the DRIFT spectra during the isotopic exchange reaction, both $C^{16}O_2$ and $C^{18}O_2$ molecular species were adsorbed on YSZ to evidence the expected wavenumbers for the vibrations of ^{16}O- and ^{18}O-containing carbonate-type species, respectively. The corresponding spectra are presented in Fig. 6. The assignments of the different IR bands obtained after the adsorption of CO_2 on YSZ was performed in agreement with the work of Köck et al. [51] who studied the adsorption of CO and CO_2 on Y_2O_3, YSZ and ZrO_2. After adsorption of 4 mbar $C^{16}O_2$, most of the IR bands observed in the 1200–1700 cm^{-1} region were attributed to the bidentate hydrogen carbonate species (b-$HC^{16}O_3^-$) with bands centred at 1640, 1429 and 1223 cm^{-1} corresponding to the ν_{as}(OCO), ν_s(OCO) and δ(OH) vibrational modes, respectively. After adsorption of 4 mbar of $C^{18}O_2$, the IR bands corresponding to the same vibrations of $HC^{18}O_3^-$ (hydrogen carbonate) compounds were detected at 1631, 1416 and 1213 cm^{-1} in agreement to the expected red isotopic shift. The appearance of these bands is consistent with the simultaneous detection of a negative signals at 3705 cm^{-1} ($C^{16}O_2$) and 3690 cm^{-1} ($C^{18}O_2$) due to the consumption of surface hydroxyl groups, and the appearance of the IR bands at 3619

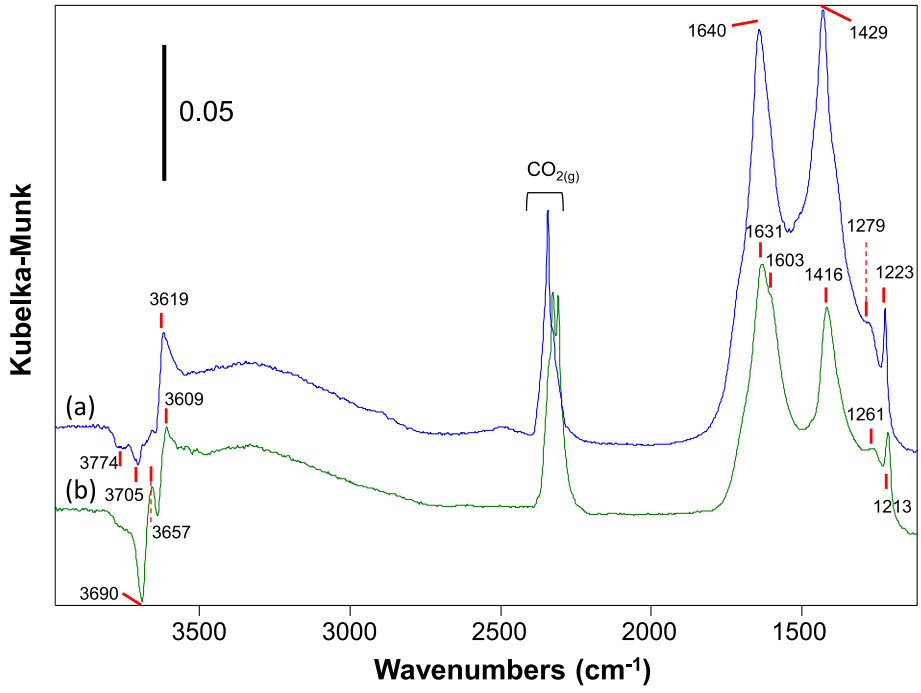

Fig. 6. DRIFT spectra collected at RT after adsorption of 4 mbar (a) $C^{16}O_2$ and (b) $C^{18}O_2$ on YSZ. These spectra were obtained after subtracting the spectra collected before CO_2 adsorption on the degassed YSZ sample.

cm^{-1} ($C^{16}O_2$) and 3609 cm^{-1} ($C^{18}O_2$) corresponding to the $\nu(^{16}OH)$ and $\nu(^{18}OH)$ stretching modes of hydrogen carbonate species, respectively. The other IR bands observed might be ascribed to monodentate hydrogen carbonate and to more strongly adsorbed bridged carbonate species; the presence of bidentate carbonate species cannot be excluded. Finally, gaseous $C^{16}O_2/C^{18}O_2$ is observed in the 2200–2400 cm^{-1} spectral range.

The IOIE experiment with $C^{18}O_2$ was then performed in the Harrick chamber of DRIFTS cell at 200 °C. The data obtained by mass spectrometry and DRIFT spectroscopy during the first 15 min of exchange are shown in **Fig. 7a** and **b**, respectively. An inset of the DRIFT spectra in the wavenumber range of 1100–1900 cm^{-1} is presented in Fig. 7c. In agreement with the TPOIE results (Fig. 5), the isotopic distribution shows that the exchange of $C^{18}O_2$ to form $C^{18}O^{16}O$ and $C^{16}O_2$ is very fast at 200 °C, so that after only 4 min of reaction the $C^{16}O_2$ becomes the predominant isotope species of CO_2 in the gas phase. The successive IR spectra collected as a function of reaction time (Fig. 7b) provided information on the nature of adsorbed species during the exchange reaction. Four bands recorded at 1212, 1404, 1433 and 1615 cm^{-1} and two negative bands at 3690 and 3640 cm^{-1}, characteristic of the monodentate and bidentate hydrogen carbonate species, respectively, resulting from the reaction of surface –OH groups with $C^{18}O_2$, were observed. The presence of carbonate species was also evidenced after a degassing step where two IR bands at 1406 and 1449 cm^{-1} (spectra not shown) persisted, characterizing more thermally stable adsorbed species.

The remarkable result is the *blue shift* of the bands observed during the reaction. This is particularly visible for the δ(OH) vibrational mode of HCO_3^- from 1212 to 1223 cm^{-1} during the first 15 min of exchange reaction. It is worth noting that a shift is observable as early as the second recorded spectrum (ca. 1 min of reaction). As explained previously, the bending modes of $^{18}O—H$ and $^{16}O—H$ groups of hydrogen carbonate species are expected at 1212 and 1223 cm^{-1}, respectively.

The present combination of DRIFTS with isotopic exchange techniques enabled to prove that the mechanism of exchange occurs on YSZ with *hydrogen carbonate* intermediate species, following Eqs. 14 and 15, and according to the mechanistic scheme shown in Fig. 8:

$$C^{18}O_{2(g)} + {}^{16}OH^-_{(ads)} \rightleftharpoons HC^{18}O_2{}^{16}O^-_{(ads)} \quad (14)$$

$$HC^{18}O_2{}^{16}O^-_{(ads)} \rightleftharpoons C^{16}O^{18}O_{(g)} + {}^{18}OH^-_{(ads)} \quad (15)$$

One can speculate, as proposed by Peri on alumina [49], that the carbonate species formed on YSZ do not participate in the exchange process because of their strong stability.

3.5. Determination of oxygen diffusion coefficient

An additional remarkable result is the demonstration of a very high oxygen mobility in the bulk of YSZ, likely governed by the presence of anionic oxygen vacancies. To the best of our knowledge, O diffusion coefficient was not reported on YSZ at low temperatures. Indeed, such a measurement is usually carried out on dense YSZ in which ionic conductivity is extremely low for temperatures below 500 °C because of the diffusion barrier generated during the sintering process.

To highlight the high oxygen diffusion suspected from previous experiments on YSZ, a comparison was made with $Ce_{0.5}Zr_{0.5}O_2$ on the basis of IOIE experiments at different temperatures. Ceria-zirconia with the

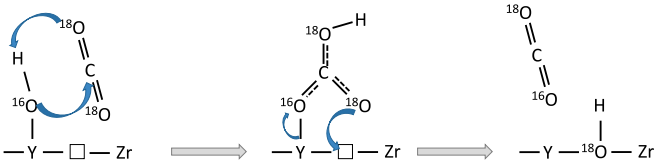

Fig. 8. Proposed oxygen exchange mechanism via hydrogen carbonate species between gas-phase CO_2 and lattice O of YSZ. Note that the O—H group may be linked to the Zr instead of Y element.

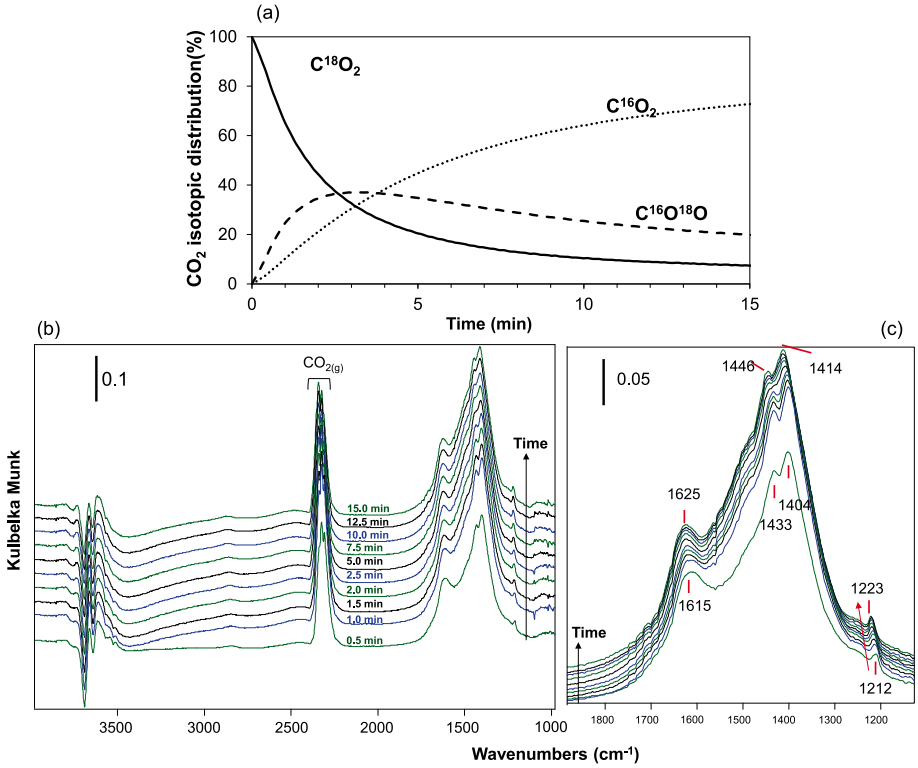

Fig. 7. Heterolytic exchange of gaseous $C^{18}O_2$ as a function of time carried out in the DRIFTS cell: (a) evolution of the CO_2 isotopic distribution on YSZ (mass spectrometry analysis); (b) DRIFT spectra collected during the first 15 min of exchange; (c) inset in the 1100–1900 cm^{-1} wavenumber region related to (b).

composition $Ce_{0.5}Zr_{0.5}O_2$ was chosen because this mixed metal oxide is known for its very interesting and important property of bulk oxygen mobility [52,53]. Efstathiou's group conducted elegant transient isothermal isotopic exchange (TIIE) experiments and $^{18}O_2$ temperature-programmed isotopic exchange studies (TPIE) for studying the kinetics of surface and bulk oxygen diffusion in this mixed oxide [54–56]. The studied sample, provided by Rhodia, has a specific surface area of 61 m^2 g^{-1} compared to 13 m^2 g^{-1} for YSZ (Table 1). Oxygen diffusion coefficients were calculated by fitting the curves of heterolytic exchange with $C^{18}O_2$, obtained under isothermal conditions between 150 and 400 °C depending on the sample. A model derived from Klier et al. [24] was used to describe the Fickian diffusion and the kinetics at the interface between the oxide surface and the gas phase. More details were given in the Experimental part.

The curves representing the evolution of the ^{18}O atomic fraction in the gas phase as a function of the square root of time are shown in Fig. 9a for YSZ, and Fig. 9b for $Ce_{0.5}Zr_{0.5}O_2$. The experimental curves are depicted with solid lines, while the fitted curves using the diffusion model are presented with dashed lines. In the case of YSZ, three experiments at 150, 200 and 250 °C were performed. Exchange experiments at higher temperatures were not evaluated because of the very high exchange rates already observed at 250 °C. The oxygen diffusion coefficients (D) determined from the fitted curves are given in Table 2. The D values increase from 3.98 × 10^{-17} cm^2 s^{-1} at 150 °C to 26.0 × 10^{-17} cm^2 s^{-1} at 250 °C. For comparison, the lowest temperature found in the literature for determining diffusion coefficient of oxygen in the same commercial YSZ material was reported by de Souza et al. [57] at 450 °C by means of $^{18}O/^{16}O$ exchange and secondary ion mass spectrometry (SIMS). At this temperature, the values varied between 4.33 × 10^{-16} cm^2 s^{-1} and 8.12 × 10^{-15} cm^2 s^{-1} depending on the model used and on the pre-treatment of the sample performed. With the D value of 12.0 × 10^{-17} cm^2 s^{-1} obtained at 200 °C, an Arrhenius plot between 150 and 250 °C enabled to calculate an apparent activation energy (Ea) of 35 kJ mol^{-1} for bulk oxygen diffusion in YSZ. On the basis of this Ea value, an extrapolation of our data at 450 °C gives a D value of 2.42 × 10^{-15} cm^2 s^{-1} which is in good agreement with those of de Souza et al. [54]. Contrary to YSZ, the evolution with time of the ^{18}O atomic fraction (α_g) is very slow for $Ce_{0.5}Zr_{0.5}O_2$ sample. The D values at 150 and 200 °C are 0.10 and 0.21 × 10^{-17} cm^2 s^{-1}, respectively, almost two orders of magnitude lower than those obtained for YSZ. IOIE experiments at higher temperatures (up to 400 °C) were performed to obtain a D value of 3.04 × 10^{-17} cm^2 s^{-1} for $Ce_{0.5}Zr_{0.5}O_2$ close to the one of YSZ at 150 °C. An extrapolation assuming an Ea of 31 kJ mol^{-1} for $Ce_{0.5}Zr_{0.5}O_2$ shows that a temperature of exchange of 660 °C would be required to have the bulk diffusion rate observed at 200 °C for YSZ. Note that approximation is made of constant Ea in the range of 200–700 °C.

Table 2
Comparison of the oxygen diffusion coefficients estimated at various temperatures for YSZ and $Ce_{0.5}Zr_{0.5}O_2$ solids.

Mixed oxide	Diffusion coefficient (10^{-17} cm^2 s^{-1})					Activation energy (kJ mol^{-1})
	150 °C	200 °C	250 °C	300 °C	400 °C	
YSZ	3.98	12.0	26.0			35
$Ce_{0.5}Zr_{0.5}O_2$	0.10	0.21	–	0.75	3.04	31

Galdikas et al. [53] reported for $Pt/Ce_{0.5}Zr_{0.5}O_2$ a bulk oxygen diffusion coefficient of 0.77 × 10^{-17} cm^2 s^{-1} at 400 °C based on $^{18}O/^{16}O$ heterolytic exchange with $^{18}O_2$. The presence of Pt particles, very active for the dissociation of molecular oxygen, permitted the measurement of bulk O diffusion with $^{18}O_2/^{16}O$ isotopic exchange. The values calculated in the present study are therefore very consistent with literature reported values and validate the utilization of $C^{18}O_2$ for the determination of oxygen diffusion coefficients at low temperatures where molecular O_2 cannot be activated in the oxide surface.

For several decades, many studies reported that methane combustion could follow the redox MvK mechanism on Pd-based catalysts [7,8]. On PdO/Al_2O_3, the lattice oxygen involved in the MvK mechanism is usually restricted to PdO cluster and does not associate support lattice oxygen [58]. When YSZ is used as a support for Pd, the methane combustion reaction has been relatively unexplored. Under specific reaction conditions (low pressure and closed recycling system), a MvK mechanism was demonstrated to oxidize CH_4 over Pd/YSZ at 425 °C [19]19. Furthermore, the investigation of single YSZ or YSZ-supported metal catalysts for other oxidation reactions (partial oxidation of methane [17,29]; propane oxidation [36]) has revealed the occurrence of the MvK mechanism over this mixed oxide. In the present study, the catalytic behaviour of Rh/YSZ and Pd/YSZ in methane combustion was compared in terms of light-off curves. A similar temperature of ignition at around 300 °C was found for both catalysts. However, the characterization techniques using labelled molecules suggest different behaviour related to the participation of lattice oxygen of YSZ. The CD_4/CH_4 equilibration reaction demonstrated that the C—H bond activation was promoted by the presence of Pd, while the heterolytic isotopic exchange with $^{18}O_2$ molecule confirmed that the dissociative activation of molecular oxygen was much more favourable on Rh than Pd. Finally, heterolytic isotopic exchange with $C^{18}O_2$ permitted to demonstrate that at the temperature where combustion begins, the diffusion of bulk oxygen from YSZ was relatively fast. All these results suggest that on Rh/YSZ, the MvK mechanism which is proposed to govern the reaction of methane combustion does not only imply oxygen atoms linked to Rh but also to YSZ's lattice O. Indeed, at the temperature of reaction which must be sufficiently high to activate the C—H bond, the bulk oxygen

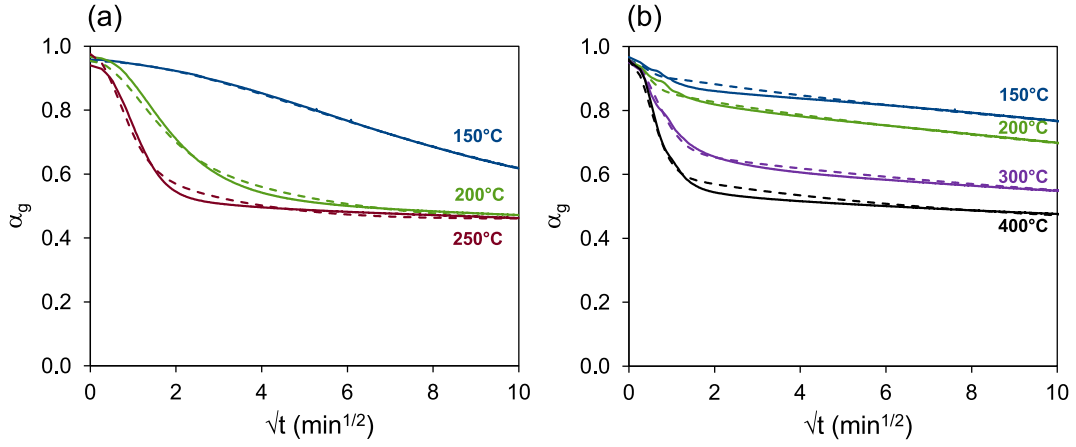

Fig. 9. Experimental (solid line) and fitted (dashed line) curves obtained by IOIE reaction with $C^{18}O_2$ at various temperatures over (a) YSZ and (b) $Ce_{0.5}Zr_{0.5}O_2$ samples.

diffusion is high enough to regenerate consumed O atoms at the surface.

This study illustrated that the utilization of labelled molecules to investigate the interaction between the gas phase and a solid catalyst via isotopic exchange reactions is powerful not only for a better understanding of a catalytic reaction (here the methane oxidation to CO_2 and H_2O) but also to improve catalyst design. Up to now the oxygen diffusion in the YSZ mixed oxide of interest for high temperature electrochemical systems was usually investigated by $^{18}O/^{16}O$ heterolytic exchange, where it was shown to be limited *below 550 °C*. In the present study, the substitution of $C^{18}O_2$ for $^{18}O_2$ was particularly relevant and efficient to reveal the high mobility of YSZ lattice O at mild temperatures. This paves the way to the design of new catalytic materials applied to reactions known to follow a MvK mechanism, such as the selective oxidation of hydrocarbons, oxidative coupling or dehydrogenation, hydrodesulfurization, and NO_x removal [14,59].

4. Conclusions

Yttria-stabilized zirconia containing 8 mol% Y_2O_3 was studied as support of Pd and Rh metals for the catalytic combustion of methane. YSZ alone is not active below 600 °C. After deposition of 0.46 wt% Rh or 0.43 wt% Pd, Rh/YSZ and Pd/YSZ catalysts exhibited very similar catalytic activities at low temperatures with the conversion of methane starting around 250 °C. In the operating feed composition reaction conditions (CH_4:O_2:He = 1:2:14), the conversion of CH_4 was complete between 525 and 700 °C over the Rh/YSZ, while Pd/YSZ showed an inhibition above 500 °C, likely due to PdO decomposition. YSZ also proved to be a much more suitable support than Al_2O_3 for Rh-based catalysts, while Pd/Al_2O_3 formulation is known as a reference for methane combustion. CD_4/CH_4 homomolecular exchange and $^{18}O_2/^{16}O_2$ heterolytic exchange revealed that the activation of C—H bond of methane is favoured on Pd/YSZ compared with Rh/YSZ, whereas Rh promoted O_2 dissociation to a larger extent than Pd. Based on $C^{18}O_2/^{16}O$ heterolytic exchange experiments performed over YSZ and $Ce_{0.5}Zr_{0.5}O_2$ solids alone, oxygen diffusion coefficients were calculated showing that the bulk oxygen diffusion in YSZ at 200 °C would be equivalent to the one measured at 660 °C in $Ce_{0.5}Zr_{0.5}O_2$. This result strongly suggests that during the CH_4 combustion reaction at low temperature, ca. 250 °C, all of the lattice oxygen of YSZ could participate in the reaction via a Mars-van Krevelen mechanism. The combination of DRIFTS and heterolytic exchange with $C^{18}O_2$ allowed to propose a mechanism for the exchange between the gas-phase CO_2 and lattice oxygen of YSZ involving hydrogen carbonate intermediate species and YSZ surface anionic vacancies.

CRediT authorship contribution statement

Alexandre Nau: Investigation. **Rémy Pointecouteau:** Investigation. **Mélissandre Richard:** Investigation, Conceptualization, Writing – review & editing. **Thomas Belin:** Supervision, Conceptualization, Writing - review & editing. **Fabien Can:** Supervision, Writing - review & editing. **Clément Comminges:** Supervision, Funding acquisition, Writing - review & editing. **Nicolas Bion:** Conceptualization, Project administration, Funding acquisition, Writing – review & editing.

Declaration of Competing Interest

The authors declare that they have no known competing financial interests or personal relationships that could have appeared to influence the work reported in this paper.

Data availability

Data will be made available on request.

Acknowledgments

The European Union (ERDF) and Région Nouvelle Aquitaine are gratefully acknowledged for their financial support.

References

[1] I.V. Provornaya, I.V. Filimonova, L.V. Eder, V.Y. Nemov, E.A. Zemnukhova, Formation of energy policy in Europe, taking into account trends in the global market, Energy Rep. 6 (2020) 599–603, https://doi.org/10.1016/j.egyr.2019.09.032.

[2] L. He, Y. Fan, J. Bellettre, J. Yue, L. Luo, A review on catalytic methane combustion at low temperatures: catalysts, mechanisms, reaction conditions and reactor designs, Renew. Sust. Energ. Rev. 119 (2020), 109589, https://doi.org/10.1016/j.rser.2019.109589.

[3] D. Jiang, K. Khivantsev, Y. Wang, Low-temperature methane oxidation for efficient emission control in natural gas vehicles: Pd and beyond, ACS Catal. 10 (2020) 14304–14314, https://doi.org/10.1021/acscatal.0c03338.

[4] I. Sharma, D. Rackemann, J. Ramirez, D.J. Cronin, L. Moghaddam, J.N. Beltramini, J. Te'o, K. Li, C. Shi, W.O.S. Doherty, Exploring the potential for biomethane production by the hybrid anaerobic digestion and hydrothermal gasification process: a review, J. Clean. Prod. 362 (2022), 132507, https://doi.org/10.1016/j.jclepro.2022.132507.

[5] S.K. Sansaniwal, M.A. Rosen, S.K. Tyagi, Global challenges in the sustainable development of biomass gasification: an overview, Renew. Sust. Energ. Rev. 80 (2017) 23–43, https://doi.org/10.1016/j.rser.2017.05.215.

[6] R.B. Jackson, S. Abernethy, J.G. Canadell, M. Cargnello, S.J. Davis, S. Féron, S. Fuss, A.J. Heyer, C. Hong, C.D. Jones, H. Damon Matthews, F.M. O'Connor, M. Pisciotta, H.M. Rhoda, R. de Richter, E.I. Solomon, J.L. Wilcox, K. Zickfeld, Atmospheric methane removal: a research agenda, Philos. Trans. R. Soc. A Math. Phys. Eng. Sci. 379 (2021), https://doi.org/10.1098/rsta.2020.0454, 20200454.

[7] Z. Tang, T. Zhang, D. Luo, Y. Wang, Z. Hu, R.T. Yang, Catalytic combustion of methane: from mechanism and materials properties to catalytic performance, ACS Catal. 12 (2022) 13457–13474, https://doi.org/10.1021/acscatal.2c03321.

[8] T.V. Choudhary, S. Banerjee, V.R. Choudhary, Catalysts for combustion of methane and lower alkanes, Appl. Catal. A Gen. 234 (2002) 1–23, https://doi.org/10.1016/S0926-860X(02)00231-4.

[9] P. Gélin, M. Primet, Complete oxidation of methane at low temperature over noble metal based catalysts: a review, Appl. Catal. B Environ. 39 (2002) 1–37, https://doi.org/10.1016/S0926-3373(02)00076-0.

[10] S. Royer, D. Duprez, F. Can, X. Courtois, C. Batiot-Dupeyrat, S. Laassiri, H. Alamdari, Perovskites as substitutes of Noble metals for heterogeneous catalysis: dream or reality, Chem. Rev. 114 (2014) 10292–10368, https://doi.org/10.1021/cr500032a.

[11] M. Monai, T. Montini, R.J. Gorte, P. Fornasiero, Catalytic oxidation of methane: Pd and beyond, Eur. J. Inorg. Chem. 2018 (2018) 2884–2893, https://doi.org/10.1002/ejic.201800326.

[12] D. Ciuparu, M.R. Lyubovsky, E. Altman, L.D. Pfefferle, A. Datye, Catalytic combustion of methane over palladium-based catalysts, Catal. Rev.-Sci. Eng. 44 (2002) 593–649, https://doi.org/10.1081/CR-120015482.

[13] H. Yoshida, T. Nakajima, Y. Yazawa, T. Hattori, Support effect on methane combustion over palladium catalysts, Appl. Catal. B Environ. 71 (2007) 70–79, https://doi.org/10.1016/j.apcatb.2006.08.010.

[14] P. Vernoux, L. Lizarraga, M.N. Tsampas, F.M. Sapountzi, A. De Lucas-Consuegra, J.-L. Valverde, S. Souentie, C.G. Vayenas, D. Tsiplakides, S. Balomenou, E. A. Baranova, Ionically conducting ceramics as active catalyst supports, Chem. Rev. 113 (2013) 8192–8260, https://doi.org/10.1021/cr4000336.

[15] M.N. Tsampas, F.M. Sapountzi, P. Vernoux, Applications of yttria stabilized zirconia (YSZ) in catalysis, Catal. Sci. Technol. 5 (2015) 4884–4900, https://doi.org/10.1039/C5CY00739A.

[16] A.G. Steghuis, J.G. van Ommen, K. Seshan, J.A. Lercher, New highly active catalysts in direct partial oxidation of methane to synthesis gas, in: M. de Pontes, R. L. Espinoza, C.P. Nicolaides, J.H. Scholtz, M.S. Scurrell (Eds.), Stud. Surf. Sci. Catal., Elsevier, 1997, pp. 403–408, https://doi.org/10.1016/S0167-2991(97)80368-0.

[17] A.G. Steghuis, J.G. van Ommen, J.A. Lercher, On the reaction mechanism for methane partial oxidation over yttria/zirconia, Catal. Today 46 (1998) 91–97, https://doi.org/10.1016/S0920-5861(98)00330-7.

[18] M. Richard, F. Can, D. Duprez, S. Gil, A. Giroir-Fendler, N. Bion, Remarkable enhancement of O_2 activation on yttrium-stabilized zirconia surface in a dual catalyst bed, Angew. Chem. Int. Ed. 53 (2014) 11342–11345, https://doi.org/10.1002/anie.201403921.

[19] M. Richard, F. Can, S. Gil, A. Giroir-Fendler, D. Duprez, N. Bion, Study of lanthanum Manganate and yttrium-stabilized zirconia-supported palladium dual-bed catalyst system for the Total oxidation of methane: a study by $^{18}O_2/^{16}O_2$ isotopic exchange, ChemCatChem. 8 (2016), https://doi.org/10.1002/cctc.201600598, 1860–1860.

[20] M. Richard, D. Duprez, N. Bion, F. Can, Investigation of methane oxidation reactions over a dual-bed catalyst system using ^{18}O labelled DRIFTS coupling, ChemSusChem. 10 (2017) 210–219, https://doi.org/10.1002/cssc.201601165.

[21] D. Duprez, Oxygen and Hydrogen Surface Mobility in Supported Metal Catalysts: Study by $^{18}O/^{16}O$ and $^{2}H/^{1}H$ Exchange, in: Isot, Published By Imperial College Press and Distributed by World Scientific Publishing Co., Heterog. Catal, 2006, pp. 133–181, https://doi.org/10.1142/9781860948084_0006.

[22] K. Klier, J. Nováková, P. Jíru, Exchange reactions of oxygen between oxygen molecules and solid oxides, J. Catal. 2 (1963) 479–484, https://doi.org/10.1016/0021-9517(63)90003-4.

[23] V.S. Muzykantov, V.V. Popovskii, G.R. Boreskov, Kinetics of isotope exchange in a molecular oxygen–solid oxide system, Kinet. Katal. 4 (1964).

[24] K. Klier, E. Kučera, Theory of exchange reactions between fluids and solids with tracer diffusion in the solid, J. Phys. Chem. Solids 27 (1966) 1087–1095, https://doi.org/10.1016/0022-3697(66)90084-9.

[25] J. Crank, The Mathematics of Diffusion, 2d ed, Clarendon Press, Oxford, [Eng], 1975.

[26] J.C. Fuentes Cabrera, C.A. Coello Coello, Handling constraints in particle swarm optimization using a small population size, in: A. Gelbukh, Á.F. Kuri Morales (Eds.), MICAI 2007 Adv. Artif, Intell., Springer, Berlin Heidelberg, Berlin, Heidelberg, 2007, pp. 41–51, https://doi.org/10.1007/978-3-540-76631-5_5.

[27] R. Poli, Analysis of the publications on the applications of particle swarm optimisation, J. Artif. Evol. Appl. 2008 (2008), e685175, https://doi.org/10.1155/2008/685175.

[28] P.-A. Répécaud, H. Kaper, M. Richard, F. Can, N. Bion, Enhancement of oxygen activation and mobility in $CaTi_xFe_{1-x}O_{3-\delta}$ oxides, ChemCatChem 9 (2017) 2095–2098, https://doi.org/10.1002/cctc.201700103.

[29] J. Zhu, J.G. van Ommen, A. Knoester, L. Lefferts, Effect of surface composition of yttrium-stabilized zirconia on partial oxidation of methane to synthesis gas, J. Catal. 230 (2005) 291–300, https://doi.org/10.1016/j.jcat.2004.09.025.

[30] R.J. Farrauto, M.C. Hobson, T. Kennelly, E.M. Waterman, Catalytic chemistry of supported palladium for combustion of methane, Appl. Catal. A Gen. 81 (1992) 227–237, https://doi.org/10.1016/0926-860X(92)80095-T.

[31] M. Delporte, H. Kaper, F. Can, N. Bion, X. Courtois, Iron-doped $CaTiO_3$ and Pd/YSZ dual bed catalytic system for CH_4 emission control from natural gas vehicle, Top. Catal. (2023), https://doi.org/10.1007/s11244-022-01777-1.

[32] X. Feng, L. Jiang, D. Li, S. Tian, X. Zhu, H. Wang, C. He, K. Li, Progress and key challenges in catalytic combustion of lean methane, J. Energy Chem. 75 (2022) 173–215, https://doi.org/10.1016/j.jechem.2022.08.001.

[33] S.H. Oh, P.J. Mitchell, Effects of rhodium addition on methane oxidation behavior of alumina-supported noble metal catalysts, Appl. Catal. B Environ. 5 (1994) 165–179, https://doi.org/10.1016/0926-3373(94)00034-4.

[34] S.H. Oh, P.J. Mitchell, R.M. Siewert, Methane oxidation over alumina-supported noble metal catalysts with and without cerium additives, J. Catal. 132 (1991) 287–301, https://doi.org/10.1016/0021-9517(91)90149-X.

[35] F. Aupretre, C. Descorme, D. Duprez, D. Casanave, D. Uzio, Ethanol steam reforming over $Mg_xNi_{1-x}Al_2O_3$ spinel oxide-supported Rh catalysts, J. Catal. 233 (2005) 464–477, https://doi.org/10.1016/j.jcat.2005.05.007.

[36] M.A. Fortunato, A. Princivalle, C. Capdeillayre, N. Petigny, C. Tardivat, C. Guizard, M.N. Tsampas, F.M. Sapountzi, P. Vernoux, Role of lattice oxygen in the propane combustion over Pt/Yttria-stabilized zirconia : isotopic studies, Top. Catal. 57 (2014) 1277–1286, https://doi.org/10.1007/s11244-014-0293-5.

[37] D. Martin, D. Duprez, Mobility of surface species on oxides. 1. Isotopic exchange of $^{18}O_2$ with ^{16}O of SiO_2, Al_2O_3, ZrO_2, MgO, CeO_2, and CeO_2-Al_2O_3. Activation by noble metals. Correlation with oxide basicity, J. Phys. Chem. 100 (1996) 9429–9438, https://doi.org/10.1021/jp9531568.

[38] R. Horn, R. Schlögl, Methane activation by heterogeneous catalysis, Catal. Lett. 145 (2015) 23–39, https://doi.org/10.1007/s10562-014-1417-z.

[39] C. Kemball, R.G.W. Norrish, Catalysis on evaporated metal films II. The efficiency of different metals for the reaction between methane and deuterium, Proc. R. Soc. Lond. Ser. Math. Phys. Sci. 217 (1997) 376–389, https://doi.org/10.1098/rspa.1953.0069.

[40] M.V. Ananyev, D.M. Zakharov, H/D isotopic exchange between methane and a proton-conducting oxide: theory and experiment, Catal, Sci. Technol. 10 (2020) 3561–3571, https://doi.org/10.1039/C9CY02566A.

[41] S. Bedrane, C. Descorme, D. Duprez, $^{16}O/^{18}O$ isotopic exchange: a powerful tool to investigate oxygen activation on $M/Ce_xZr_{1-x}O_2$ catalysts, Appl. Catal. A Gen. 289 (2005) 90–96, https://doi.org/10.1016/j.apcata.2005.04.016.

[42] D.H. Lenz, Wm C. Conner, Computer analysis of the cracking patterns of deuterated hydrocarbons, Anal. Chim. Acta 173 (1985) 227–238, https://doi.org/10.1016/S0003-2670(00)84960-0.

[43] J. Au-Yeung, K. Chen, A.T. Bell, E. Iglesia, Isotopic studies of methane oxidation pathways on PdO catalysts, J. Catal. 188 (1999) 132–139, https://doi.org/10.1006/jcat.1999.2643.

[44] P. Mars, D.W. van Krevelen, Oxidations carried out by means of vanadium oxide catalysts, Chem. Eng. Sci. 3 (1954) 41–59, https://doi.org/10.1016/S0009-2509(54)80005-4.

[45] M. Kilo, C. Argirusis, G. Borchardt, R.A. Jackson, Oxygen diffusion in yttria stabilised zirconia—experimental results and molecular dynamics calculations, Phys. Chem. Chem. Phys. 5 (2003) 2219–2224, https://doi.org/10.1039/B300151M.

[46] E.Kh. Kurumchin, M.V. Perfiliev, An isotope exchange study of the behaviour of electrochemical systems, Solid State Ionics 42 (1990) 129–133, https://doi.org/10.1016/0167-2738(90)90001-8.

[47] J. Kim, H. Ha, W.H. Doh, K. Ueda, K. Mase, H. Kondoh, B.S. Mun, H.Y. Kim, J. Y. Park, How Rh surface breaks CO_2 molecules under ambient pressure, Nat. Commun. 11 (2020) 5649, https://doi.org/10.1038/s41467-020-19398-1.

[48] S. Sharma, S. Hilaire, J.M. Vohs, R.J. Gorte, H.-W. Jen, Evidence for oxidation of ceria by CO_2, J. Catal. 190 (2000) 199–204, https://doi.org/10.1006/jcat.1999.2746.

[49] J.B. Peri, Oxygen exchange between carbon dioxide (oxygen-18) and acidic oxide and zeolite catalysts, J. Phys. Chem. 79 (1975) 1582–1588, https://doi.org/10.1021/j100582a023.

[50] B. Bachiller-Baeza, P. Ferreira-Aparicio, A. Guerrero-Ruiz, I. Rodríguez-Ramos, Oxygen exchange between $C^{18}O_2$ and basic metal oxides (CaO, MgO, ZrO_2, ZnO), in: C. Li, Q. Xin (Eds.), Stud. Surf. Sci. Catal, Elsevier, 1997, pp. 277–284, https://doi.org/10.1016/S0167-2991(97)80847-6.

[51] E.-M. Köck, M. Kogler, T. Bielz, B. Klötzer, S. Penner, In situ FT-IR spectroscopic study of CO_2 and CO adsorption on Y_2O_3, ZrO_2, and Yttria-stabilized ZrO_2, J. Phys. Chem. C 117 (2013) 17666–17673, https://doi.org/10.1021/jp405625x.

[52] Y. Madier, C. Descorme, A.M. Le Govic, D. Duprez, Oxygen mobility in CeO_2 and $Ce_xZr_{(1-x)}O_2$ compounds: study by CO transient oxidation and $^{18}O/^{16}O$ isotopic exchange, J. Phys. Chem. B 103 (1999) 10999–11006, https://doi.org/10.1021/jp991270a.

[53] A. Galdikas, C. Descorme, D. Duprez, F. Dong, H. Shinjoh, Study of the oxygen diffusion on three-way catalysts: a kinetic model, Top. Catal. 30–31 (2004) 405–409, https://doi.org/10.1023/B:TOCA.0000029782.78561.47.

[54] S.Y. Christou, H. Bradshaw, C. Butler, J. Darab, A.M. Efstathiou, Effect of thermal aging on the transient kinetics of oxygen storage and release of commercial $CexZr_{1-x}O_2$-based solids, Top. Catal. 52 (2009) 2013–2018, https://doi.org/10.1007/s11244-009-9402-2.

[55] S.Y. Christou, M.C. Álvarez-Galván, J.L.G. Fierro, A.M. Efstathiou, Suppression of the oxygen storage and release kinetics in $Ce_{0.5}Zr_{0.5}O_2$ induced by P, ca and Zn chemical poisoning, Appl. Catal. B Environ. 106 (2011) 103–113, https://doi.org/10.1016/j.apcatb.2011.05.013.

[56] S.Y. Christou, A.M. Efstathiou, The effects of P-poisoning of $Ce_xZr_{1-x}O_2$ on the transient oxygen storage and release kinetics, Top. Catal. 56 (2013) 232–238, https://doi.org/10.1007/s11244-013-9959-7.

[57] R.A.D. Souza, M.J. Pietrowski, U. Anselmi-Tamburini, S. Kim, Z.A. Munir, M. Martin, Oxygen diffusion in nanocrystalline yttria-stabilized zirconia: the effect of grain boundaries, Phys. Chem. Chem. Phys. 10 (2008) 2067–2072, https://doi.org/10.1039/B719363G.

[58] H. Stotz, L. Maier, A. Boubnov, A.T. Gremminger, J.-D. Grunwaldt, O. Deutschmann, Surface reaction kinetics of methane oxidation over PdO, J. Catal. 370 (2019) 152–175, https://doi.org/10.1016/j.jcat.2018.12.007.

[59] J.R.H. Ross, Chapter 7 - the kinetics and mechanisms of catalytic reactions, in: J.R. H. Ross (Ed.), Contemp. Catal, Elsevier, Amsterdam, 2019, pp. 161–186, https://doi.org/10.1016/B978-0-444-63474-0.00007-2.